Electronic Supplementary Information for

High sensitivity and automatic chemiluminescence detection of glucose and lactate using a spin-disc paper-based device

Wenqiang Tong,[ac] Jiaming Shi,[ac] Zhihang Yu,[ac] Bin Ran,[ac] Huaying Chen*[bc] and Yonggang Zhu *[bc]

[a.] School of Science, Harbin Institute of Technology, Shenzhen, Shenzhen 518055, China

[b.] School of Mechanical Engineering and Automation, Harbin Institute of Technology, Shenzhen, Shenzhen 518055, China

[c.] Center for Microflows and Nanoflows, School of Mechanical Engineering and Automation, Harbin Institute of Technology, Shenzhen, Shenzhen 518055, China

* Correspond authors: chenhuaying@hit.edu.cn； zhuyonggang@hit.edu.cn；

2. Materials and methods

2.1 Chemicals and materials

The D- (+)-glucose and sodium L-lactate were purchased from Sigma Aldrich (St. Louis, USA). The luminol, p-iodophenol (PIP), phosphate buffer solution (PBS, 1X, pH7.2-7.4), Tris–HCl buffer solution (TBS) (1.0M, pH9.0), horseradish peroxidase (HRP) and glucose oxidase (GO_X) were bought from Shanghai Macklin Biochemical Co., Ltd. (Shanghai, China). The hydrogen peroxide (H_2O_2), Hydrochloric acid (HCl), and Sodium hydroxide (NaOH) were obtained from Aladdin Reagent Co., Ltd. (Shanghai, China). The pH of the tris buffer solution (0.05-0.4mM) was adjusted to 7- 10.5 using either HCl (0.1M) or NaOH (0.4M). The lactate oxidase (LO_X) was procured from Shanghai yuan ye Bio-Technology Co., Ltd. (Shanghai, China). The artificial sweat and saliva were bought from Shenzhen Zhong Wei Instrument Co., Ltd. (Shenzhen, China). The fetal bovine serum (FBS), trypsin, and Penicillin-Streptomycin Solution (100X) were acquired from Corning Corporation (New York, U.S.A). The F-12K Medium (Kaighn's Modification of Ham's F-12 Medium, X702KJ, No glucose) and PC3 prostate cancer cells were purchased from iCell Bioscience Inc. (Shanghai, China). A live/dead assay kit (Calcein AM/PI) and the filter paper (Whatman Grade 1) were obtained from Shanghai Zeye Bio-Technology Co., Ltd. (Shanghai, China) and GE Healthcare Worldwide (Shanghai, China), respectively. All reagents were of analytical grade and used without further purification. Ultrapure water was always employed for solution preparation.

2.2 The top and bottom paper fabrication

The wax rings with an inner/outer diameter of 6/15 mm (top paper) and 3/17 mm (bottom paper) were fabricated on filter paper to form flow barriers. The inner regions were used for loading either sample or reaction reagents. The wax rings were printed using a wax printer (Xerox Colorqube 8570), before being heated at 150°C for 3 minutes using a hot plate (ASONE, Japan). Then the PET transparent film was punched with 8 mm holes and then laminated on one side of the top paper to allow the sample region to be uncovered using a laminator (Deli 3895) at 120°C. The bottom paper was also laminated using a whole PET film at the same temperature. Then the rings of the top and bottom paper dishes were cut and respectively attached to the holes on the chip carriers and the bottom holders using double-sided tape.

2.3 Study of the detection conditions

The luminescence intensity of the spin-disc paper device is influenced by the substances during the chemiluminescence reaction. The glucose and lactate in the sample were oxidized to H_2O_2 using glucose oxidase (GOx) and lactate oxidase (LOx), respectively. Afterward, the luminol, a readily oxidizable compound, was oxidized by H_2O_2 generated by samples in the alkaline solution with enzyme (HRP) and PIP. Therefore, in this paper, the pH (7-10.5), the concentration of luminol (5-20mM), and the quantity of catalysts such as PIP (5-20mM), HRP (25-20U/mL), GO_X(10-120U/mL), and LO_X (10-70U/mL) were studied to acquire maximal CL signal.

To explore the impact of various pH levels (ranging from 7 to 10.5) in tris buffer solution (TBS) on luminescence intensity, we adjusted TBS (0.3 mM) using HCl (0.1 M) or NaOH (0.4 M). The probe substrates (luminol - 15.0 mM, PIP - 2.0 mM, HRP - 125 U/mL) were then prepared with different pH TBS. A pre-embedded 1 μL substrate was placed in the bottom paper's detection zone. Subsequently, 7 μL of the sample (H_2O_2 0.1 mM) was added to the top paper's sample area. Activating the device, we monitored the fluorescence signal through a PMT, and based on signal strength, determined the optimal TBS pH.

To assess the impact of substance concentrations within the probe substrate (luminol, PIP, HRP) on luminescence intensity, the substrate was dissolved in pH 9.5 TBS at 0.3 mM. A detection sample of 7 μL of 0.1 mM H_2O_2 was used. For the effect of luminol concentration, the probe substrate in PBS included luminol (5-20 mM), PIP (2.0 mM), and HRP (125 U/mL).For PIP's effect on luminescence, the TBS probe substrate comprised luminol (10 mM), varying PIP (0-3.0 mM), and constant HRP (125 U/mL). In the case of HRP's effect, the TBS probe substrate had luminol (10 mM), PIP (2.0 mM), and HRP concentration (25-200 U/mL). After preparing the probe substrate, 1 μL was placed in the detection area of the bottom paper. Then, 7 μL of the sample (0.1 mM H_2O_2) was added to the top paper's sample area. The device was run, and PMT tracked the luminescence signal. Concentrations of luminol, PIP, and HRP were chosen based on the signal strength.

Glucose (0.1 mM) and lactate (0.1 mM) were utilized as detection samples to investigate the impact of GO_X and LOX concentrations on luminescence intensity. The substrate (luminol 10 mM, PIP 2.0 mM, HRP 150 U/mL) was dissolved in TBS at pH 9.5 with a concentration of 0.3 mM. GO_X was prepared in PBS at concentrations ranging from 10 to 100 U/mL, while LO_X was prepared at concentrations from 10 to 70 U/mL. Following this, 5 μL of enzyme solution and 1 μL of substrate were pre-embedded into the sample area of the top paper and the detection area of the bottom paper, respectively. Once the pre-embedded reagents had dried, 7 μL of the sample was introduced to the sample area of the top paper. The device was operated, and the luminescence signal was tracked using a PMT. Subsequently, the appropriate GO_X and LO_X concentrations were determined based on the magnitude of the generated luminescence signal.

2.4 Characterization of the detection capability

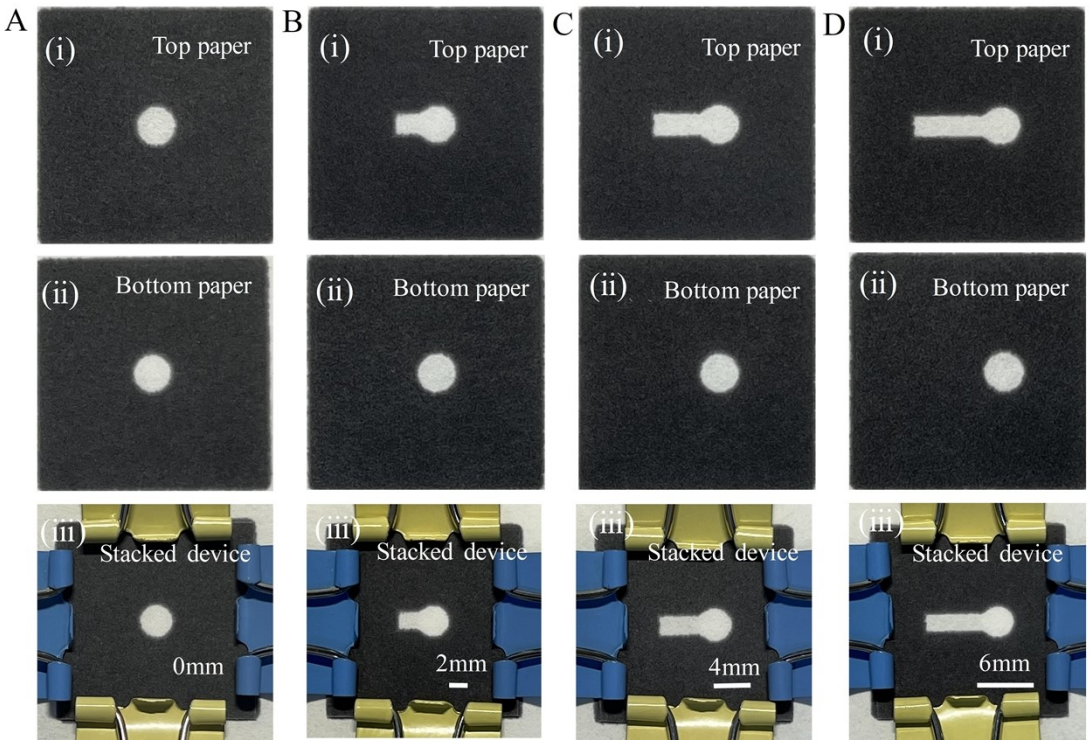

Fig. S1. The in-situ reaction device (A), and the lateral flow devices with different channel lengths (B-D).

2.5 Storage stability study of the reagents for CL assay

The stability of the substrate reagent was invested since it was significant for the practical application and advancement of the devices. The substrate reagent containing luminol, PIP, and HRP was stored in a fridge at 4 ˚C for 20 days. One μL reagent containing luminol (10 mM), PIP (2.0 mM), and HRP (150 U/mL) was loaded to the detection zone of the bottom paper for the CL response of 7μL 0.1mM H_2O_2 every other day.

2.6 Interference study of the spin-disc device CL assay

The selectivity of the fabricated spin-disc device was further investigated by using ascorbic acid (AA), glutamate, fructose, maltose, uric acid (UA), potassium chloride (KCl), and sodium chloride (NaCl) as typical interferences. The chemiluminescent response of glucose (0.1mM), lactate (0.1mM), and the typical interferences (0.1mM) were tested, respectively.

3. Results and discussion

3.1 Study of the detection conditions

Luminol and H_2O_2-mediated chemiluminescence (CL) reactions exhibit enhanced efficacy in alkaline environments. Consequently, a comprehensive examination of the influence of CL reagent pH becomes imperative. Fig. S2. A (black line) suggested that CL drastically augmented and decreased as the pH increased from 7 to 9.5 and from 9.5 to 10.5, respectively. The low CL intensity was related to the limited dissolving of luminol at a pH lower than 8[1]. Fig. S2. A (red line) revealed that the CL did not significantly vary when the luminol concentration increased from 5 to 10 mM (P=0.075). However, it drastically decreased by 53% as the concentration of luminol further raised from 10 to 20 mM. This phenomenon might be related to the self-quenching effect, which was more pronounced when the luminol concentration was higher[2]. Moreover, the PIP was added to the detection region as the signal enhancer[3]. The black curve in Fig. S2. B indicated that the CL intensity increased to the maximum at the PIP concentration of 2.0mM and then dramatically decreased with the increase of PIP concentration. The decrease in CL intensity at higher PIP concentration was reported as a result of the increase in non-radiative transition leading to a decrease in luminescence intensity[4]. Lastly, CL intensity increased as the raise of HRP concentration and reached a maximum at the concentration of 150 U/mL (see Fig. S2. B red line).

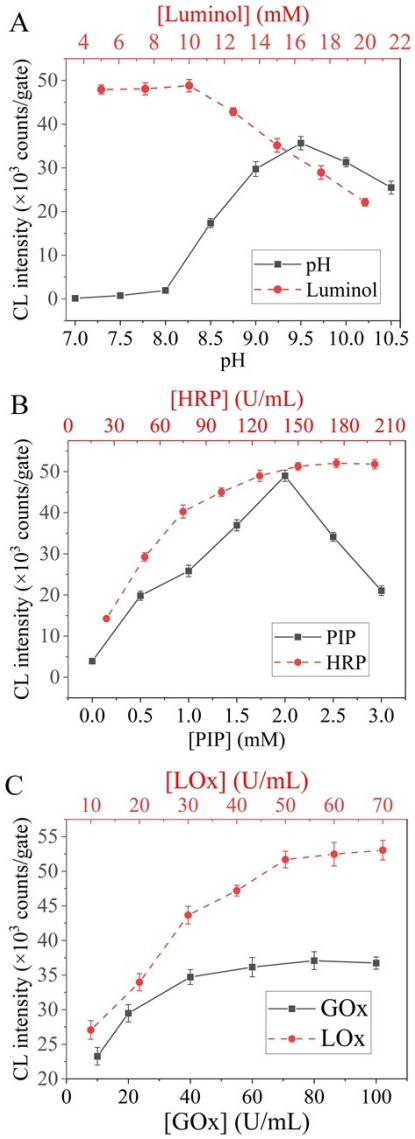

Fig. S2. The study of detection conditions. The influence of (A) the pH of TBS, and the luminol concentration, (B) the concentration of PIP and HRP, (C) the concentration of GOx and LOx on the CL intensity.

The optimal concentration of GOx and LOx was also studied to obtain maximal CL intensity. The CL intensity gradually increased as the GOx concentration increased to 60 U/mL and became constant at larger GOx concentrations (see Fig. S2. C (black line)). Similarly, CL intensity increased to the maximum when the LOx concentration was 50 U/mL and dropped as the concentration raised further(Fig. S2. C (red line)). Therefore, the concentration of 60 U/mL and 50 U/mL was employed for GOx and LOx, respectively.

3.2 Storage stability of the detection reagents

The stability of detection reagents is crucial for their practical application and further development. In this study, the stability was evaluated by monitoring the CL response of detection using the reagents for 20 days, as demonstrated in Fig. S3. The paper chips were stored at room temperature and covered to prevent any potential interference when not in use. The results revealed that the CL intensity only varied slightly in 20 days, as illustrated in Figure S3. Specifically, after 10 and 20 days, the device maintained 98.9% and 94.9% of its initial response, respectively ($P > 0.05$). These findings indicate that the device exhibited excellent storage stability and may be suitable for long-distance transportation to remote areas.

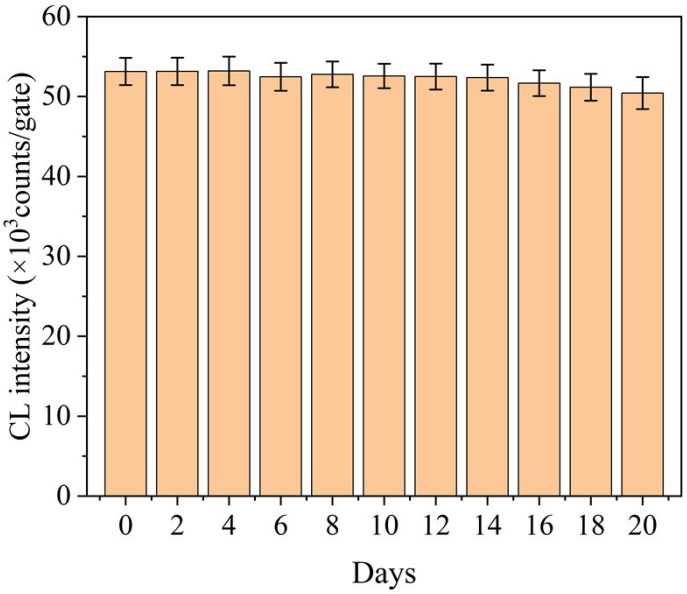

Fig. S3. Storage stability of the reagents for the determination of H_2O_2. Assay conditions: PBS (1X, pH 7.2-7.4), TBS (pH 9.5, 0.3 mM), [luminol]-10.0 mM, [PIP]-2.0 mM, [HRP]-150 U/mL, [H_2O_2]-0.1mM, [incubation time]-5 min, H_2O_2/Substrate solution volume-7μL/1μL. Error bars indicate the standard deviation of 3 independent measurements.

3.3 Selectivity of the spin-disc device CL assay

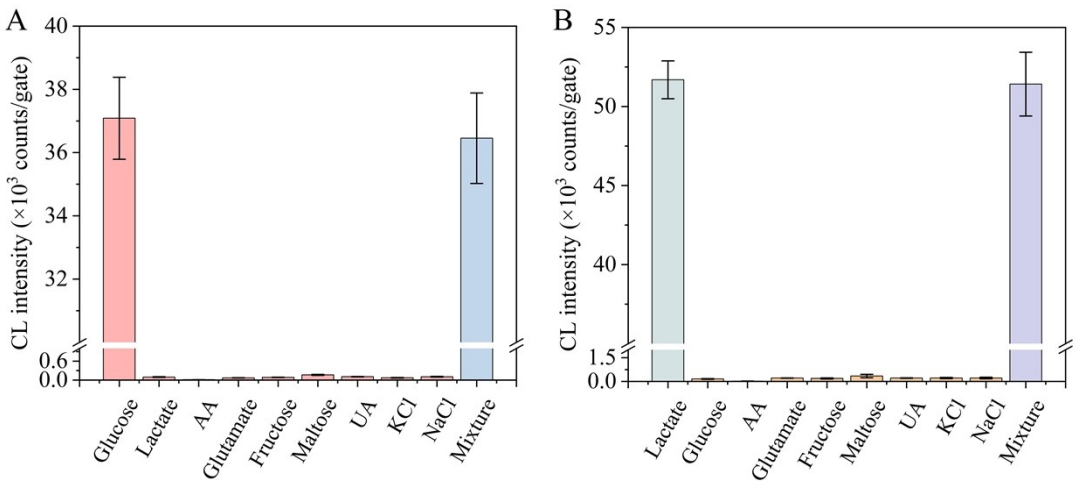

Fig. S4. Interference study of the spin-disc device. The CL intensity was measured in the presence of glucose (A), lactate (B), and various compounds including 0.1mM glucose, lactate, ascorbic acid (AA), glutamate, fructose, maltose, uric acid (UA), potassium chloride (KCl), sodium chloride (NaCl), and a mixture of glucose, lactate, and interferences. Error bars indicate the standard deviation of 3 independent measurements.

3.4 Detection of glucose and lactate

Table S1. The quantity and concentration of the various reagents

Sample	**Sample volume**	**Substrate solution**	**Substrate volume**	**Enzyme solution**	**Enzyme volume**
PBS	7 μL	Luminol-10mM	1 μL	GO_X-60 U/mL or LO_X-50 U/mL	5 μL
Sweat	7μL (glucose)/0.5 μL (lactate)	PIP-2mM			
Saliva	7 μL	HRP-150 U/mL			
Cell media	1 μL				

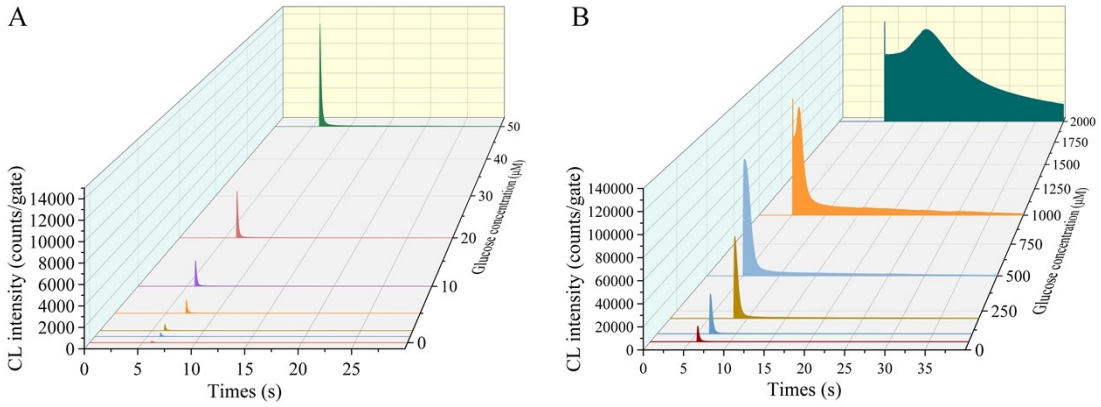

Fig. S5. Assays of glucose using the spin-disc paper devices. (A) The CL intensity over time for glucose concentrations from 0-50 μM. (B) The CL intensity over time for glucose concentrations from 50-2000 μM.

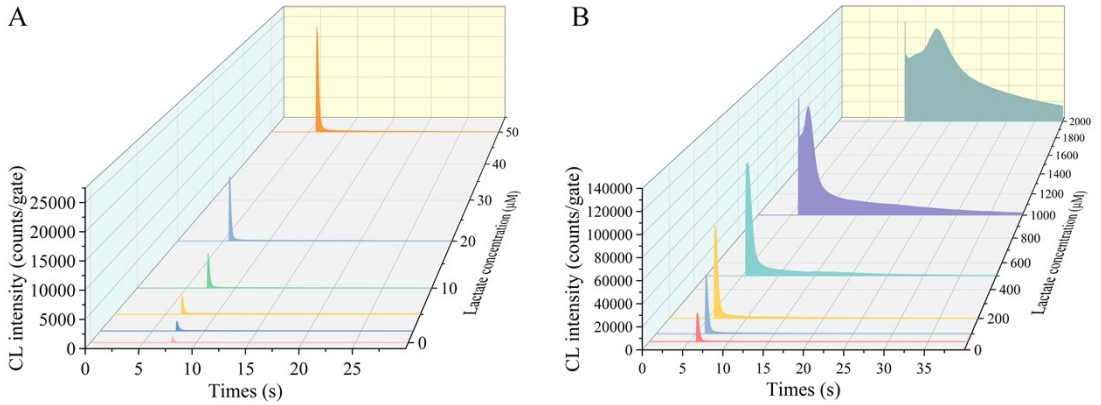

Fig. S6. Assays of lactate using the spin-disc paper devices. (A) The CL intensity over time for lactate concentrations from 0-50 μM. (B) The CL intensity over time for lactate concentrations from 50-2000 μM.

Table S2. The linear regression models for glucose and lactate determination in various samples

Sample	**Target**	**Range (μM)**	**Linear regression models**	R^2
PBS	Glucose	1.0-50	$y=0.24C_g+0.11$	0.997
		50-1000	$y=89.24\log C_g-138.60$	0.993
	lactate	2.0-50	$y=0.49C_l+0.96$	0.987
		50-1000	$y=76.88\log C_l-100.51$	0.981
Artificial	Glucose	2.0-100	$y=0.094C_{gsw}+0.13$	0.991
sweat		100-1500	$y=97.11\log C_{gsw}-182.63$	0.993
	lactate	30-1000	$y=0.023C_{lsw}+0.21$	0.959
		1000-20000	$y=74.79\log C_{lsw}-195.66$	0.981
Artificial	Glucose	1.0-50	$y=0.17C_{gsa}+0.12$	0.967
saliva		50-1000	$y=86.49\log C_{gsa}-138.4$	0.996
	lactate	2.0-50	$y=0.53C_{lsa}+0.71$	0.989
		50-1000	$y=71.51\log C_{lsa}-91.91$	0.993
Cell	Glucose	20-500	$y=15C_{gf12k}+0.3$	0.995
culture		500-10000	$y=93.8\log C_{gf12k}+36.4$	0.996
media	lactate	20-500	$y=36.5C_{lf12k}+1.06$	0.998
		500-10000	$y=87\log C_{lf12k}+46.9$	0.992

Table S3. Chemiluminescence microfluidic devices for the detection of glucose and lactate

No.	Metabolites	Method	Sample volume (μL)	Detection range (μM)	Limit of detection (μM)	Author
1	glucose	3D-printed chip	50	50-10000	20	[5]
2	glucose	μPADs	10	0-250	10	[6]
3	glucose	μPADs	2	10–1000	8	[7]
4	glucose	Cloth-CL	15	10–10000	9.74	[8]
5	glucose	Cloth-CL	10	100-100000	94.8	[4]
6	glucose	μPADs	30	420-50000	140	[9]
7	**glucose**	**μPADs**	**7**	**1.0-1000**	**0.34**	**This work**
1	lactate	μPADs	2	20–5000	15	[7]
2	lactate	3D-printed chip	15	100–20000	100	[10]
3	**lactate**	**μPADs**	**7**	**2.0-1000**	**0.3**	**This work**

Table S4. The μPADs for glucose and lactate detection in sweat

NO.	Target	Range (μM)	LOD (μM)	Method	Author
1	glucose	20-3800	0.0096	electrochemical	[11]
2	glucose	80-1250	17.05	electrochemical	[12]
3	glucose	500-2000	5.0	electrochemical	[13]
4	glucose	10-250	-	Optical	[14]
5	glucose	10-5000	4.0	Optical	[15]
6	glucose	200-2000	46	Optical	[16]
7	glucose	100-800	44	Optical	[17]
8	glucose	10-125	-	Optical	[18]
9	**glucose**	**2.0-100/100-1500**	**0.37**	**Optical**	**This work**
1	lactate	1000-50000	0.02	electrochemical	[11]
2	lactate	300-20300	3.73	electrochemical	[12]
3	lactate	2000-25000	-	Optical	[14]
4	lactate	5000-30000	1580	Optical	[16]
5	lactate	100-1000	69	Optical	[17]
6	lactate	5000-20000	-	Optical	[18]
7	lactate	10000-30000	60	Optical	[19]
8	**lactate**	**30-1000/1000-20000**	**13.30**	**Optical**	**This work**

Table S5. The μPADs for glucose and lactate detection in saliva

NO.	Target	Range (μM)	LOD (μM)	Method	Author
1	glucose	20-270	-	electrochemical	[20]
2	glucose	28-850	-	electrochemical	[21]
3	glucose	55.6-888.89	20.56	Optical	[22]
4	glucose lactate	5-50 2.5-20	2.6 0.814	Optical	[23]
5	glucose	100-10000	47	Optical	[24]
6	glucose	0-1000	29.65	Optical	[25]
7	glucose	0-2000	27	Optical	[26]
8	**glucose** **lactate**	**1-50/50-1000** **2-50/50-1000**	**0.3** **0.45**	**Optical**	**This work**

3.5 Detection of cell metabolites

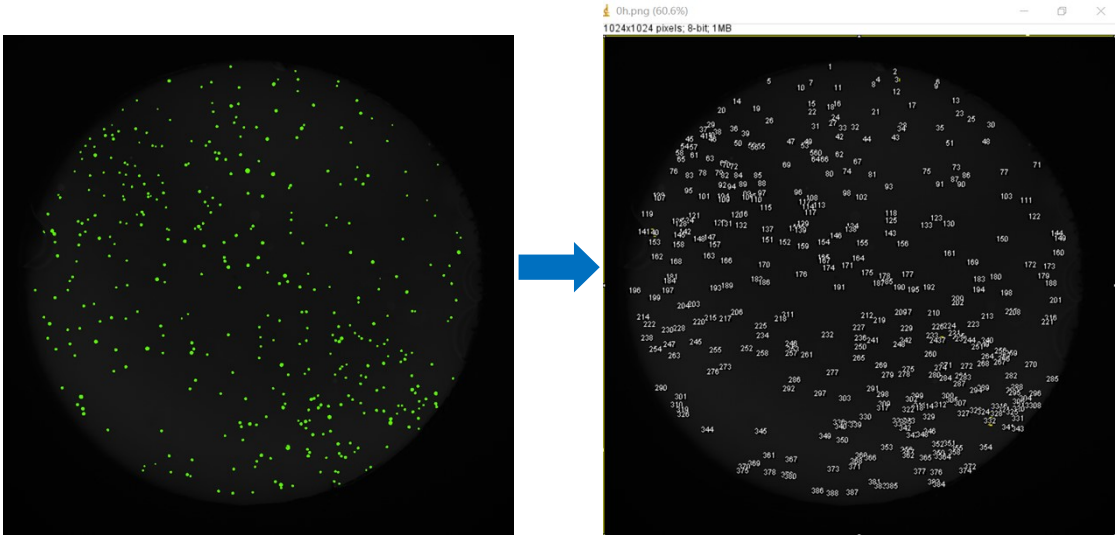

Fig. S7. Recognition of the number of cells using ImageJ.

Video S1: The working process of the spin-disc paper-based device.

Video S2: Chemiluminescence variation with time on the spin-disc paper-based device.

Video S3: Chemiluminescence variation with time on later flow device (channel length 2mm).

Video S4: Chemiluminescence variation with time on in-situ detection device.

Reference：

1. Moon BU, de Vries MG, Westerink BHC, Verpoorte E. Development and characterization of a microfluidic glucose sensing system based on an enzymatic microreactor and chemiluminescence detection. Sci China Chem 2012, **55**(4)**:** 515-523.
2. Preuschoff F, Spohn U, Blankenstein G, Mohr K-H, Kula M-R. Chemiluminometric hydrogen peroxide sensor for flow injection analysis. Fresenius' Journal of Analytical Chemistry 1993, **346**(10-11)**:** 924-929.
3. Whitehead TP, Moseley SB, Kricka LJ, Thorpe GH. Phenols as enhancers of the chemiluminescent horseradish peroxidase-luminol-hydrogen peroxide reaction: application in luminescence-monitored enzyme immunoassays. Clinical Chemistry 1985, **31**(8)**:** 1335-1341.
4. Li H, Liu C, Wang D, Zhang C. Chemiluminescence cloth-based glucose test sensors (CCGTSs): A new class of chemiluminescence glucose sensors. Biosens Bioelectron 2017, **91:** 268-275.
5. Al Lawati HAJ, Hassanzadeh J, Bagheri N. A handheld 3D-printed microchip for simple integration of the H_2O_2-producing enzymatic reactions with subsequent chemiluminescence detection: Application for sugars. Food Chem 2022, **383:** 132469.
6. Calabria D, Zangheri M, Trozzi I, Lazzarini E, Pace A, Mirasoli M, Guardigli M. Smartphone-Based Chemiluminescent Origami microPAD for the Rapid Assessment of Glucose Blood Levels. Biosensors (Basel) 2021, **11**(10).
7. Li F, Liu J, Guo L, Wang J, Zhang K, He J, Cui H. High-resolution temporally resolved chemiluminescence based on double-layered 3D microfluidic paper-based device for multiplexed analysis. Biosens Bioelectron 2019, **141:** 111472.
8. Li HJ, Wang D, Liu CL, Liu R, Zhang CS. Facile and sensitive chemiluminescence detection of H_2O_2 and glucose by a gravity/capillary flow and cloth-based low-cost platform. Rsc Advances 2017, **7**(68)**:** 43245-43254.
9. Yu J, Ge L, Huang J, Wang S, Ge S. Microfluidic paper-based chemiluminescence biosensor for simultaneous determination of glucose and uric acid. Lab Chip 2011, **11**(7)**:** 1286-1291.
10. Roda A, Guardigli M, Calabria D, Calabretta MM, Cevenini L, Michelini E. A 3D-printed device for a smartphone-based chemiluminescence biosensor for lactate in oral fluid and sweat. Analyst 2014, **139**(24)**:** 6494-6501.
11. Poletti F, Zanfrognini B, Favaretto L, Quintano V, Sun J, Treossi E, Melucci M, Palermo V, Zanardi C. Continuous capillary-flow sensing of glucose and lactate in sweat with an electrochemical sensor based on functionalized graphene oxide. Sensors and Actuators B: Chemical 2021, **344**.
12. Li M, Wang L, Liu R, Li J, Zhang Q, Shi G, Li Y, Hou C, Wang H. A highly integrated sensing paper for wearable electrochemical sweat analysis. Biosens Bioelectron 2021, **174:** 112828.
13. Cao Q, Liang B, Tu T, Wei J, Fang L, Ye X. Three-dimensional paper-based microfluidic electrochemical integrated devices (3D-PMED) for wearable electrochemical glucose detection. RSC Advances 2019, **9**(10)**:** 5674-5681.
14. Cheng Y, Feng S, Ning Q, Li T, Xu H, Sun Q, Cui D, Wang K. Dual-signal readout paper-based wearable biosensor with a 3D origami structure for multiplexed analyte detection in

sweat. Microsyst Nanoeng 2023, **9:** 36.

15. Zheng J, Zhu M, Kong J, Li Z, Jiang J, Xi Y, Li F. Microfluidic paper-based analytical device by using Pt nanoparticles as highly active peroxidase mimic for simultaneous detection of glucose and uric acid with use of a smartphone. Talanta 2022, **237**.
16. Yue X, Xu F, Zhang L, Ren G, Sheng H, Wang J, Wang K, Yu L, Wang J, Li G, Lu G, Yu H-D. Simple, Skin-Attachable, and Multifunctional Colorimetric Sweat Sensor. ACS Sensors 2022, **7**(8)**:** 2198-2208.
17. Gunatilake UB, Garcia-Rey S, Ojeda E, Basabe-Desmonts L, Benito-Lopez F. TiO2 Nanotubes Alginate Hydrogel Scaffold for Rapid Sensing of Sweat Biomarkers: Lactate and Glucose. ACS Applied Materials & Interfaces 2021, **13**(31)**:** 37734-37745.
18. Choi J, Bandodkar AJ, Reeder JT, Ray TR, Turnquist A, Kim SB, Nyberg N, Hourlier-Fargette A, Model JB, Aranyosi AJ, Xu S, Ghaffari R, Rogers JA. Soft, Skin-Integrated Multifunctional Microfluidic Systems for Accurate Colorimetric Analysis of Sweat Biomarkers and Temperature. ACS Sensors 2019, **4**(2)**:** 379-388.
19. Vaquer A, Barón E, de la Rica R. Wearable Analytical Platform with Enzyme-Modulated Dynamic Range for the Simultaneous Colorimetric Detection of Sweat Volume and Sweat Biomarkers. ACS Sensors 2020, **6**(1)**:** 130-136.
20. Kuppuswamy GP, Shabanur Matada MS, Marappan G, Mulla MY, Velappa Jayaraman S, Di Natale C, Sivalingam Y. NiOX Template-Grown Ni-MOF-Coated Carbon Paper Electrode Embedded Extended Gate Field Effect Transistor for Glucose Detection in Saliva: En Route toward the Noninvasive Diagnosis of Diabetes Mellitus. ACS Applied Electronic Materials 2023, **5**(6)**:** 3268-3279.
21. Bihar E, Wustoni S, Pappa AM, Salama KN, Baran D, Inal S. A fully inkjet-printed disposable glucose sensor on paper. npj Flexible Electronics 2018, **2**(1).
22. Mirzaei Y, Gholami A, Sheini A, Bordbar MM. An origami-based colorimetric sensor for detection of hydrogen peroxide and glucose using sericin capped silver nanoparticles. Scientific Reports 2023, **13**(1).
23. Rossini EL, Milani MI, Lima LS, Pezza HR. Paper microfluidic device using carbon dots to detect glucose and lactate in saliva samples. Spectrochimica Acta Part A: Molecular and Biomolecular Spectroscopy 2021, **248**.
24. Mercan ÖB, Kılıç V, Şen M. Machine learning-based colorimetric determination of glucose in artificial saliva with different reagents using a smartphone coupled μPAD. Sensors and Actuators B: Chemical 2021, **329**.
25. Gölcez T, Kiliç V, Şen M. A Portable Smartphone-based Platform with an Offline Image-processing Tool for the Rapid Paper-based Colorimetric Detection of Glucose in Artificial Saliva. Analytical Sciences 2020, **37**(4)**:** 561-567.
26. de Castro LF, de Freitas SV, Duarte LC, de Souza JAC, Paixão TRLC, Coltro WKT. Salivary diagnostics on paper microfluidic devices and their use as wearable sensors for glucose monitoring. Analytical and Bioanalytical Chemistry 2019, **411**(19)**:** 4919-4928.